Atomic force microscopy investigation of nano-scale roughness and wettability in middle to high rank coals, with samples from Qinshui Basin, China

Yuejian Lu[a,b,c], Dameng Liu[a,b], Yidong Cai[a,b], Changjing Gao[a,b],Qifeng Jia[a,b], Yingfang Zhou[c,d]

[a] *School of Energy Resources, China University of Geosciences, Beijing 100083, PR China*

[b] *Coal Reservoir Laboratory of National Engineering Research Center of Coalbed Methane Development & Utilization, Beijing 100083, PR China*

[c] *School of Engineering, FN263, King's College, University of Aberdeen, AB24 3UE Aberdeen, UK*

[d] *Department of Energy Resources, University of Stavanger, Stavanger, 4021, Norway*

Abstract：Coal wettability plays important role in multiphase fluids flow in coal formation including pore scale distribution of gas and water, the fluid flow velocity and drainage efficiency, which thus has a significant effect on the coalbed methane (CBM) production. In this work, we collected 17 coals with different ranks from Qinshui basin, North China and Junggar basin, Northwest China; the pore structures, mechanical properties and wettability (macroscopic and microscopic contact angle) were studied with nanodrops vapor condensation measurements and atomic force microscopy (AFM). The results show there is a negative relationship between the contact angle and roughness due to the change of adsorption sites, which is consistent with Wenzel model. The negative correlation trend between adhesive force and wettability of coal should be related to the minerals and oxygen-containing groups, the more hydrophilic of coal, the high content of –OOH and hydrophilic mineral in coal. Contact angle is largely determined by nanodrop size based on the AFM technology. Furthermore, the line tension on the surface of coal is 2.52×10-11 J/m,

drop size less than 10 nm are most heavily affected by line tension. Line tension is negligible when research the imbibition process in micropores and mesopores, and fluid flow behavior in fractures scarcely influenced by line tension. This work could provide new insights into the interactions between water molecules and coal pore surface, and provide a basis for the optimization of favorable areas in CBM reservoirs.

Keywords: AFM, pore structure, wettability, coalbed methane, line tension

1. Introduction

Coalbed methane (CBM), as a form of clean unconventional natural gas resource, is generated from coal and stored in coal seams[1,2]. The wettability of coal is an important fluid-rock property that influences interfacial interaction of fluids (methane and formation water) and coal matrix, and it represents the ability of a certain fluid to wet a solid surface [3]. As presented previously that wettability plays a vital role in the exploitation of CBM[4–6]. The production of CBM involves gas and water flow in coal formation. The wettability of coal is one of the key factors that controls gas-water distribution in pore and fracture system, capillary force, and relative permeability[7–9]. Previous scholars studied the pore distribution and wetting mechanism of coal and other rocks experimentally, such as inverse gas chromatography[10] and Nuclear magnetic resonance (NMR)[9,11], and numerically, such as the in-situ wettability determination based on high resolution fluid-rock imaging[12,13] and intel-molecular simulations [14,15].

Wettability is an important property of a solid surface and is controlled by the

chemical composition (or surface free energy) of the solid surface, the surface geometry and surface roughness [14–17]. Zhao et al. analyzed surface morphology and pore structure of coal with AFM and found the results is closed to the SEM results [18] Li et al. researched the change of roughness of coal with numerical solution[19]. The effect of surface roughness on wettability was first considered by the well-known Wenzel model [20]. In the Wenzel model, geometric construction of materials' surface is responsible for the hydrophobicity. For hydrophilic sample，with increasing solid surface roughness, macroscopic apparent contact angle turns more small. The Wenzel model is adopted to characterize the relationship between the physical structure and wettability, whereas, this model has some limitations, including limitations at the nanoscale, and ignore liquid volume stored in the asperities [21,22]. After that, the improved Wenzel models were used to describe the hydrophobic behavior of nanostructured surface. The surface fluorination treatments experiment showed that the contact angle of solid is increased with the specific surface area [23]. Furthermore, the effect of roughness on hydrophobicity has been detailed explored [24], which shows that the wettability changes with roughness from energy viewpoint. Previous NMR and X-ray photoelectron spectroscopy experiments results demonstrated that coal wettability highly depends on surface functional groups, especially oxygen-containing groups [14,25–27]. The adhesive force of coal surface could reflect surface energy, which have a great effect on wettability of coal, it is necessary to research the adhesive force of coal. Li et al. investigated that the adhesive force of coal is ranges from 20 and 50 nN [28]. Tian et al. found there is great variation between coal

samples in adhesive force value, which has a wide range of 30-400 nN [29].There are other factors controlling coal wettability including clay minerals, fluid composition, temperature, pressure, and coal rank, among of which are the function of coal wettability. However, these studies fail to reveal the intrinsic wetting mechanism of coals.

Apart from the factors above associated with wettability, there are some properties could affect wettability of materials are negligible at the microscale and play a key role in microscopic system, such as line tension[17], which is dominated by three interfacial or surface tensions and represent excess free energy relevant to per unit length of the contact line [30]. The sign and value of line tension have a great influence on wettability, positive sign indicating the length of three phase contact line tends to decrease, and resulting in increasing the contact angle, negative sign indicating the length of three phase contact line is appeared to the trend of increase, resulting in decreasing the contact angle [31]. Ma et al.[32] calculated the line tension of coal (5.01×10^{-11} J/m) based on molecular dynamics simulation, however, very limited experiment has focused on line tension in CBM system.

In this work, we analyzed the surface topography and mechanical properties of coal with AFM and affecting factors of wettability at macro and micro scales. Firstly, the roughness, pore size distribution, and high-resolution mechanical distribution of coal is obtained by surface morphology. Then we analyzed the characteristic of roughness and adhesive force and their effects on coal wettability (contact angle). Finally, the line tension of coal was calculated based on vapor condensation and then estimated

the macroscopic contact angle based on the modified Young's equation, which then compared with the contact angle measured from sessile drop method. Our results demonstrated that AFM could be effectively used to evaluate the interfacial characteristics of coal, and it would be favorable for understanding the intrinsic factors controlling the wettability of coals.

2. Materials, Experiments and Methodologies

2.1. Materials

To analysis the surface morphology and nanomechanical properties, 17 coal samples of various rank were collected from the Qinshui basin, North China and Junggar basin, Northwest China: 2 low-rank (sample B2 and B14) 2 high-rank (sample B3 and B12) and 13 medium-rank (sample B1,B4,B5,B6,B7,B8,B9,B10,B11,B13,B15,B16,B17) . During the process of AFM experiment, surface information of material was obtained based on the atomic interaction between the tip of the probe and the surface of the coal sample, this has extremely high requirements on the surface flatness of the sample being tested. According to the sample pretreatments requirement [33], the collected coal samples were cut with size of 10 mm×10 mm×3 mm and then were polished for imaging by using argon ion milling. The surface morphology and nanomechanical properties of pretreated coal samples were carried out using a Multimode 8 AFM with the PFQNM mode.

Table1 Characteristics of coal samples.

Sample No.	Proximate analysis (%)					Mineral content (%)					
	$R_{o,m}$	M_{ad}	A_{ad}	V_{ad}	FC_{ad}	Q	Ca	Do	Si	Py	Clay
B1	1.86	0.96	9.92	12.87	76.25	/	/	/	/	/	/
B2	0.56	1.46	6.94	42.13	49.47	0	13	24	63	0	0
B3	2.35	1.03	10.09	15.56	73.32	/	/	/	/	/	/

B4	1.46	0.88	11.25	22.75	65.12	/	/	/	/	/	/
B5	1.74	0.69	12.74	13.39	73.18	0	11	10	0	0	79
B6	1.84	0.69	16.09	17.29	65.93	0	60	18	2	3	17
B7	1.26	1.56	14.12	30.86	53.46	/	/	/	/	/	/
B8	1.88	0.65	9.36	23.87	66.12	7	56	16	0	0	21
B9	1.99	0.97	11.88	12.91	74.24	9	22	10	0	0	59
B10	1.54	0.68	11.3	15.65	72.37	/	/	/	/	/	/
B11	1.76	0.88	10.9	11.96	76.26	0	14	26	0	0	60
B12	2.05	1.05	8.04	8.84	82.07	0	0	13	0	3	84
B13	1.38	0.78	11.32	25.21	62.69	/	/	/	/	/	/
B14	0.62	1.72	3.9	33.57	60.81	0	23	34	43	0	0
B15	1.68	1.32	7.54	13.42	77.72	/	/	/	/	/	/
B16	1.23	0.68	12.57	22.89	63.86	/	/	/	/	/	/
B17	1.72	0.69	15.86	16.65	66.8	/	/	/	/	/	/

Note: $R_{o,m}$-maximum vitrinite reflectance; M_{ad}-moisture (air-dried basis); A_{ad}-ash content (airdried basis); V_{ad}-volatile content (air-dried basis); FC_{ad}-fixed carbon (air-dried basis); Q-Quartz; Ca-Calcite; Do-Dolomite; Si-Siderite; Py-Pyrite.

2.2 Experiments

2.2.1 AFM experiment

AFM is a powerful tool of scanning probe microscopy by recording the interaction of a sharp probe with the sample surface and has been widely used to study the surface characterization of materials in various fields [34,35]. Previously, AFM has been used to achieve surface morphology, mechanical properties, surface charge distribution of cell at the nano scale[36]. Generally, there are several imaging modes including PeakForce Tapping™, TappingMode™, Contact Mode and PhaseImaging™. In this work, PeakForce QNM mode was adopted to study morphology and mechanical properties of coal surface. Contact Mode was used to measure the shape of nanodrops on the coal surface. Before measure mechanical property of sample with AFM, choose a suitable probe and calibrations are indispensable steps, experimental and data processing procedures are the same as presented in previous work[37]. During the AFM experiment, a force-distance curve is first obtained through PeakForce Tapping technology in the PFQNM mode, then, the curve could be fitted and analyzed by the

DMT model, and the quantitative nanomechanical properties of the sample could be carried out during the scan[18]. Fig.1a shows the experimental principle of AFM, interaction force between tip and surface of material is presented as a function of distance is presented in Fig 1b.

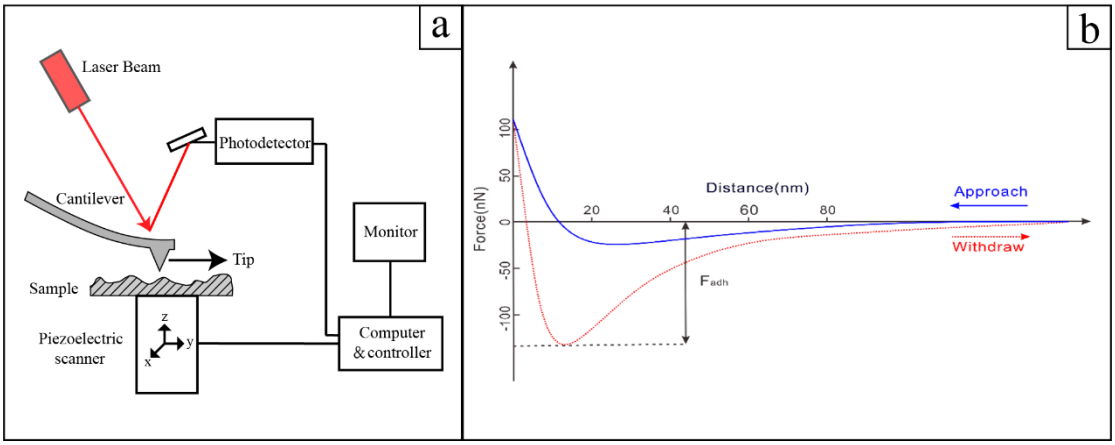

Fig.1. Basic work principle of AFM (a: Experimental principle, b: Schematic curve of force versus distance under the PeakForce QNM mode).

2.2.2 Macroscopic contact angle measurement

Contact angle was measured by using the sessile drop method, which is a common to characterize the wettability of materials. Before commencing measurements, it is necessary to check whether the sample surface is contaminated. For each sample, less than 4mg droplet of deionized water was deposited randomly on a polished coal surface at 25 Celsius [34]. Meanwhile, the shapes of droplet on the surface were record by contact angle meter (JC2000D), and the measurements were repeated 3 times for each coal sample at same experimental conditions, please refer to detailed experiment setup and procedure in our previous work [35].

2.2.3 Line tension

Macroscopic contact angle could be represented as the relationship between the surface tension of solid-liquid, liquid-gas and solid-gas, which is expressed by the

Young's equation as follows:

$$\cos\ \theta_{\infty} = \frac{\gamma_{SC} - \gamma_{SL}}{\gamma_{LC}} \qquad (1)$$

This equation is later modified by Boruvka [40] to account for line tension at microscale, as shown in Eq. (2):

$$\gamma_{SG} = \gamma_{SL} + \gamma_{LG}\cos\ \theta + \frac{\tau}{r_B} \qquad (2)$$

Combining Eq. (1) and Eq. (2), which give us the relationship between microscale and macroscale contact angle:

$$\cos\ \theta = \cos\ \theta_{\infty} - \frac{\tau}{\gamma_{LG}}\frac{1}{r_B} \qquad (3)$$

where γ_{SG}, γ_{SL} and γ_{LG} are the surface tension of solid-gas phase, solid-liquid and liquid-gas phase, respectively. τ is the apparent line tension, θ and θ_{∞} are the contact angles of a droplet of contact radius r and a macroscopic droplet, respectively.

The formation of stable nanodrops on coal surfaces for wetting studies is not a trivial task, sample B7 was firstly put into the container and increase vapor pressure until drops are in thermodynamic equilibrium with their vapor phase, then nanodrops were formatted via vapor condensation with contact angle ranging from ~7.8° to ~12.7° as shown in Fig.2. The advantages of vapor condensing method are that (a) nanodrops could evenly distribute on the surface of coal for measurement, (b) reducing the rate of water evaporation and nanodrops could remain stable.

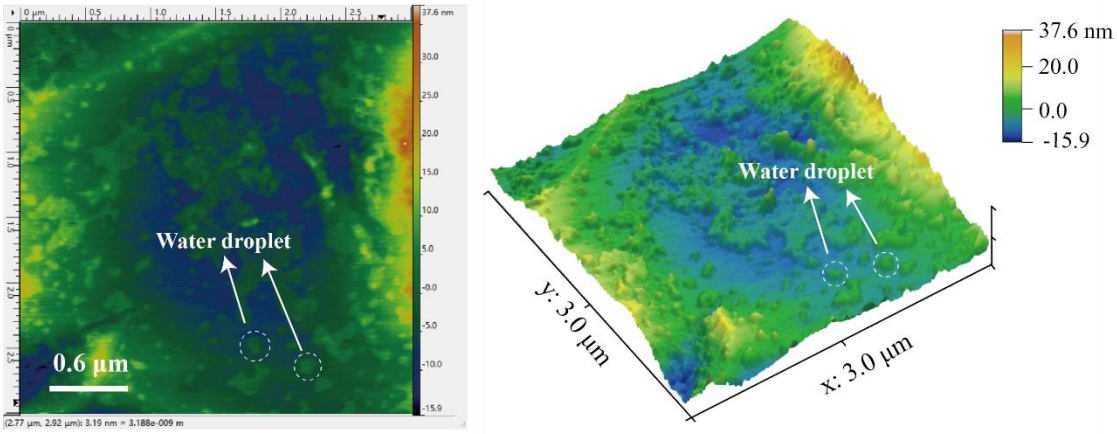

(a) (b)

Fig.2 AFM image of nanodrops on the surface of coal sample. (a) 2D image, (b)3D image (For the purpose of illustration, there is different scale in x-axis, y-axis direction and z-axis direction)

2.3 Methodologies

2.3.1 Pore morphology analysis

Before analyzing the surface topography with AFM data, the noise produced in the imaging should be removed with Flatten method [41]. Fig.3 shows the 2D surface image of sample B1 before (top) and after (bottom) flatten processing respectively. As shown in this figure, the image was processed with Flatten method show more surface information of coal, meanwhile, more surface topography changes and pore structure could be distinguished, such as clustered pores are visible in some areas as show Fig.3d.

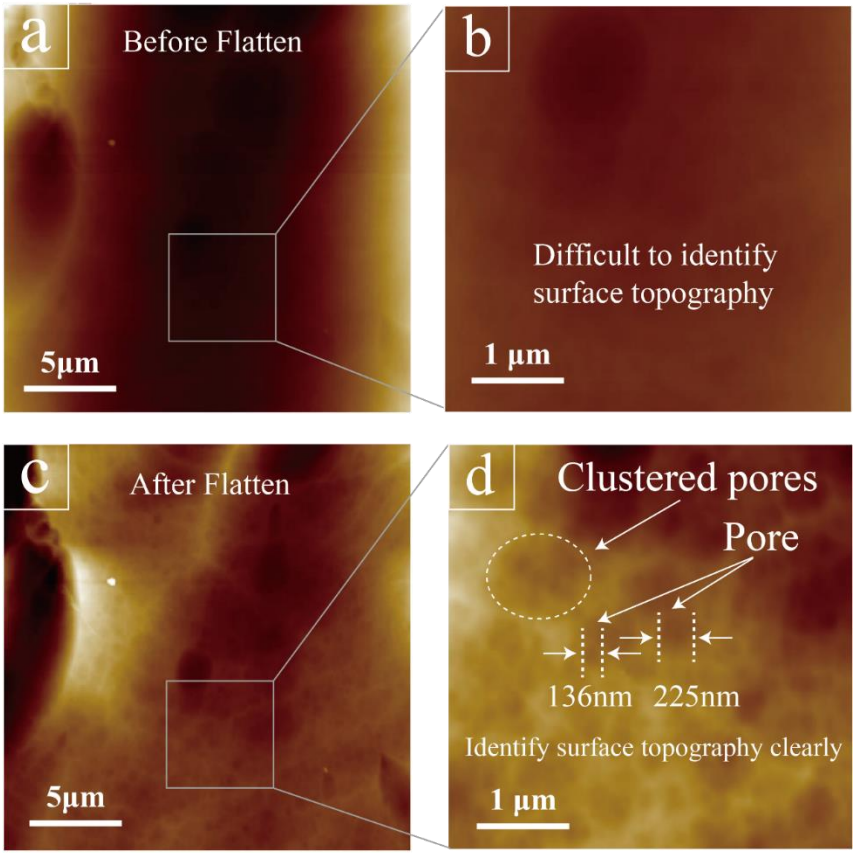

Fig.3. 2D surface image of sample B1. Top: before flatten and bottom: after Flatten

Pore heterogeneity of various rank coals is evaluated by surface morphology using NanoScope analysis and pore size distribution obtained through Gwyddion package [5]. Before AFM experiment, Argon ion milling is firstly required to prepare the samples for imaging. The “Section Analysis” module can be used for line analysis (see Fig.4a and Fig.4b) to identify the pore size and pore depth. Fig.4c shows the surface morphology of Sample B2 along the profile line. To better reflect the pore size distribution, the height value of sample surface is analyzed. Secondly, Gwyddion software is used to obtain the true pore size and its distribution. In generally, thresholding method and watershed methods are two main methods to characteristic the pore structure, thresholding method mask pore based on low height values, in addition, boundaries of pores present high slope and curvature values, which is mostly

suitable for materials with simple pore structure [5,42]. The watershed method is normally used to determinate local minima and image segmentation during image processing, which is based on water flows to part of area with the local minima. Compared to thresholding method, more pore parameters could be obtained with watershed mothed, including the pore radius, porosity, specific surface area, and pore volume [43,44], which is suitable for materials with strong heterogeneity. By comparison, watershed method could be used more effectively for pore marking of coal in this work.

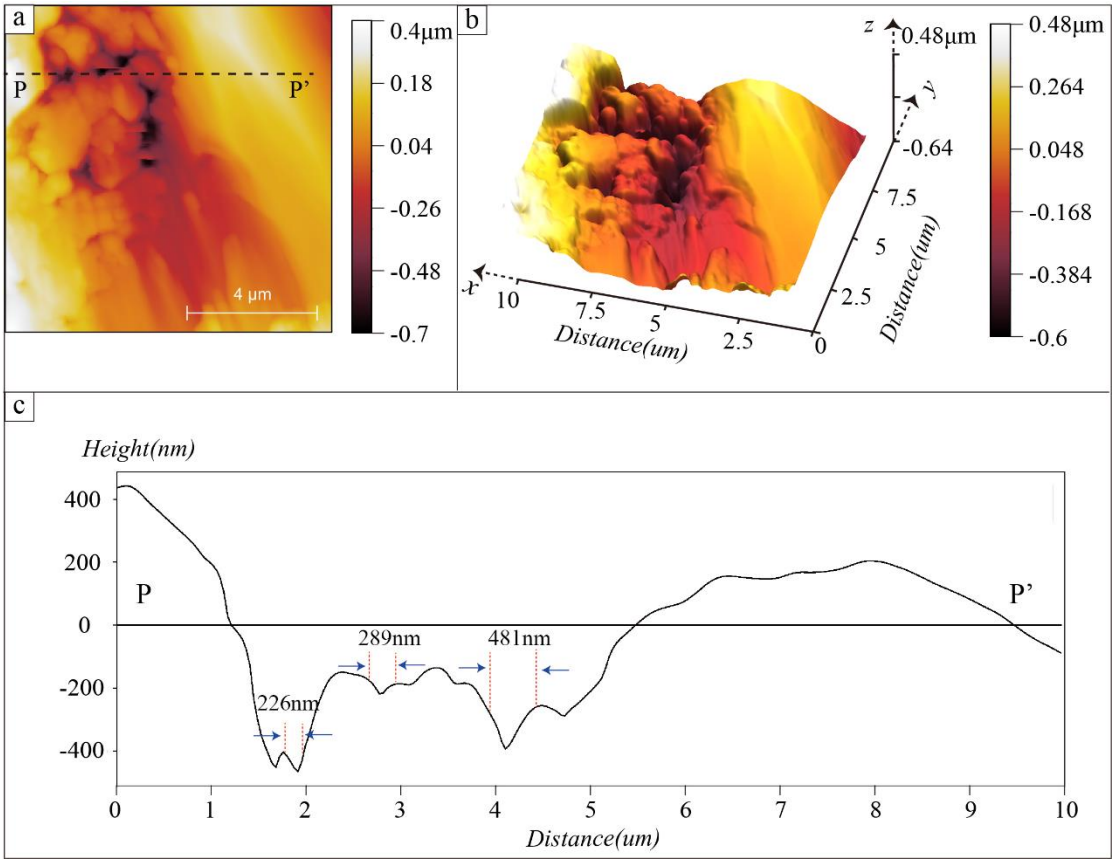

Fig. 4. Section analysis of AFM images (Section Line of Sample B3 in Fig.3a; Fig.3a, Two-dimensional map; Fig.3b three- dimensional AFM images; Fig.3c, section analysis).

2.3.2 Roughness and adhesive force analysis

Previously, surface roughness of porous material has been evaluated by the mean roughness (R_a) and root mean square roughness (R_q) [28,45]. R_a is defined as the

average absolute deviation from the mean line over one sampling length of the surface roughness, R_q indicates the standard deviation of the distribution of surface heights，which could be calculated as following[28,31,46].

$$R_a = \frac{1}{N_x N_y}\sum_{i=1}^{N_x}\ \sum_{j=1}^{N_y}\ |z(i,j) - z_{mean}| \quad (4)$$

$$R_q = \sqrt{\frac{1}{N_x N_y}\sum_{i=1}^{N_x}\sum_{j=1}^{N_y}(z(i,j) - z_{mean})^2} \quad (5)$$

Where:

$$z_{mean} = \frac{1}{N_x N_y}\sum_{i=1}^{N_x}\ \sum_{j=1}^{N_y} Z_{ij} \quad (6)$$

N_x and N_y mean the number of points on the x-axis and y-axis, respectively.

The surface adhesion of coal is obtained from AFM in the Peakforce imaging mode. The surface adhesion of the coal was counted by NanoScope. The DMT Model is then used to obtain the force-distance by fitting the Retract part of the force- distance curve using the equation proposed by [47] as given below:

$$F_{tip} = \frac{4}{3}E^*\sqrt{Rd^3} + F_{adh} \quad (7)$$

Where F_{tip} is the tip-sample force，nN. R is the tip radius, nm. d is the sample deformation, nm. F_{adh} is the adhesive force during the contact, nN. E* denotes reduced modulus and it could be calculated as follow:

$$E^* = \left(\frac{1-v_s^2}{E_s} + \frac{1-v_{tip}^2}{E_{tip}}\right)^{-1} \quad (8)$$

Where v_s is Poisson's ratio of the sample, v_{tip} is Poisson's ratio of the probe, and E_{tip} is Young's modulus of the tip material. Here in this experiment reported, the Poisson's ratio of the coal was assumed to be 0.3 [48].

3 Results

3.1 Pore morphology and structure

The AFM images of 10 coal samples were first segmented with watershed method. The segmented images of several selected samples (B4, B6, B7, B9) are presented in Fig.5. As shown in this figure, the pore space is labeled with blue. The segmented images were then used to obtain the pore size, number of pores, total pore volume and mean pore size using “Gain statistics” module in Gwyddion, these results are summarized in Table 2. Similar to previously study[49], five types of pore have been identified in this work, these are super micropores (<2 nm), micropores (2-10 nm), mesopores (10-10^2), macropores (10^2-10^3), super macropores (10^3-10^4), and microfractures (>10^4 nm). Coal sample with different location marked variation of pore distribution and show high heterogeneity, micropores and mesopores are two main pore types developed among the coal samples except sample B2 and B7. The percentage of micro-mesopore ranges from 42.2%-92.7%, the higher the percentage of this type pore, the stronger affinity to CH_4, and is favorable for CBM enrichment[49]. The number of pores in sample B10 and B10 are 1-2 orders of magnitude higher than the other samples, which are 1392 and 1942 respectively (Fig.5a). In general, the sample with a larger number of pores has higher porosity. The porosity of coals varies from 3.49% to 11.72%. Pore size distribution are represented by the waveform characteristics, the kurtosis values vary from 2.7 to 5.19, and the skewness values changes from 4.89 to 27.28. Moreover, detailed observations on pore structure could be found based on segmented AFM image, there are two types pore in

coal matrix based on pore genesis and distribution characteristics [50], including mineral associated pores (Fig.5c) and organic matter pores (Fig.5d). The detailed pore matrix characterization could help us to under coal facies and paleo-environmental conditions better and then provide a basis to optimize CBM producation.

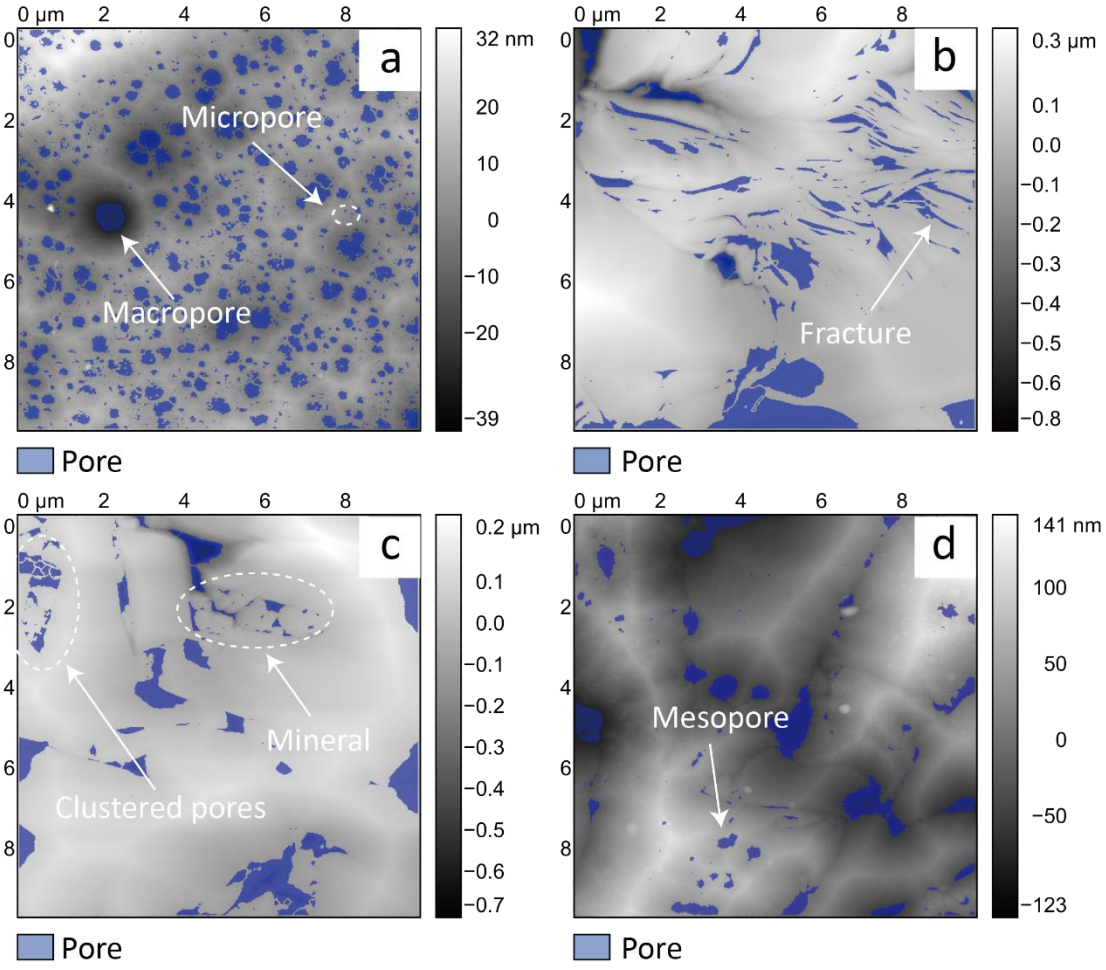

Fig.5. Segmentation results of pore distribution of 4 coal samples with Watershed method. (a) Sample B4, micropores are developed; (b) Sample B6, fractures are developed with good connectivity; (c) Sample B7, clustered pores could be segmented clearly; (d) Sample B9, strong heterogeneity of pore distribution

255 Table 2. Pore parameters of different coals obtained from segmented AFM images

Sample	Count of pores	TPV	Porosity	MPS	Percentage			Ku	Skew
					Micro-mesopore	Macropore	Super macropore		
B1	24	0.06	5.35%	243.1	78.4%	16.2%	5.4%	2.7	5.79
B2	86	0.26	3.49%	140.5	42.2%	56.7%	1.1%	2.33	4.86
B3	146	0.052	10.18%	107.1	86.1%	13.7%	0.2%	3.95	13.79
B4	1392	0.167	11.72%	63.25	74.4%	25.6%	0%	5.19	27.28
B5	236	0.075	8.54%	80.86	82.2%	16.95%	0.85%	4.43	17.72
B6	379	0.252	7.01%	74.61	76.19%	23.28%	0.53%	4.45	18.73
B7	148	0.389	5.59%	108	57.4%	41.2%	1.4%	3.5	11.32
B8	117	0.158	7.89%	155	63.25%	35.04%	1.71%	2.938	8.028
B9	243	0.103	6.813%	81.8	80.66%	18.52%	0.82%	4.25	16.72
B10	1942	0.034	10.39%	46.67	92.7%	7.05%	0.25%	3.85	12.54

256 Note: TPV-Total pore volume, μm3; MPS-Mean pore size, nm; Ku- Pore kurtosis; Skew-Pore skewness

3.2 Surface roughness of coal

The two-dimensional maps and three-dimensional roughness of the coal samples are shown in Fig.6. As shown in this figure, surface topography of the presented four samples varies significantly. The roughness profile of a given direction is selected to characterize the change of surface morphology of coals intuitively (Fig.6-a3, Fig.6-b3, Fig.6-c3 and Fig.6-d3). Samples could be classified into two distinct types based on the morphology of coal surface：developed and undeveloped pore. A large number of gas related pores are widely developed in sample B4 and B9, as shown in Fig.6-a3 and Fig.6-d3, these pores are relatively isolated with poor connectively. High degree of surface roughness is observed in sample B9 with surface height is more than 30 nm, while the surface height of B4 is around 10 nm. In addition, it clearly shows that there are a lot of pores in B6 and B7 sample with good connectivity, big gap in vertical height could be found with ranging from -203.5 nm to 63.8 nm for B4 sample and ranging from -248.7 nm to 138.5 nm for B7 sample, that is, this kind of coal are favorable for CBM flow in opposite to adsorption.

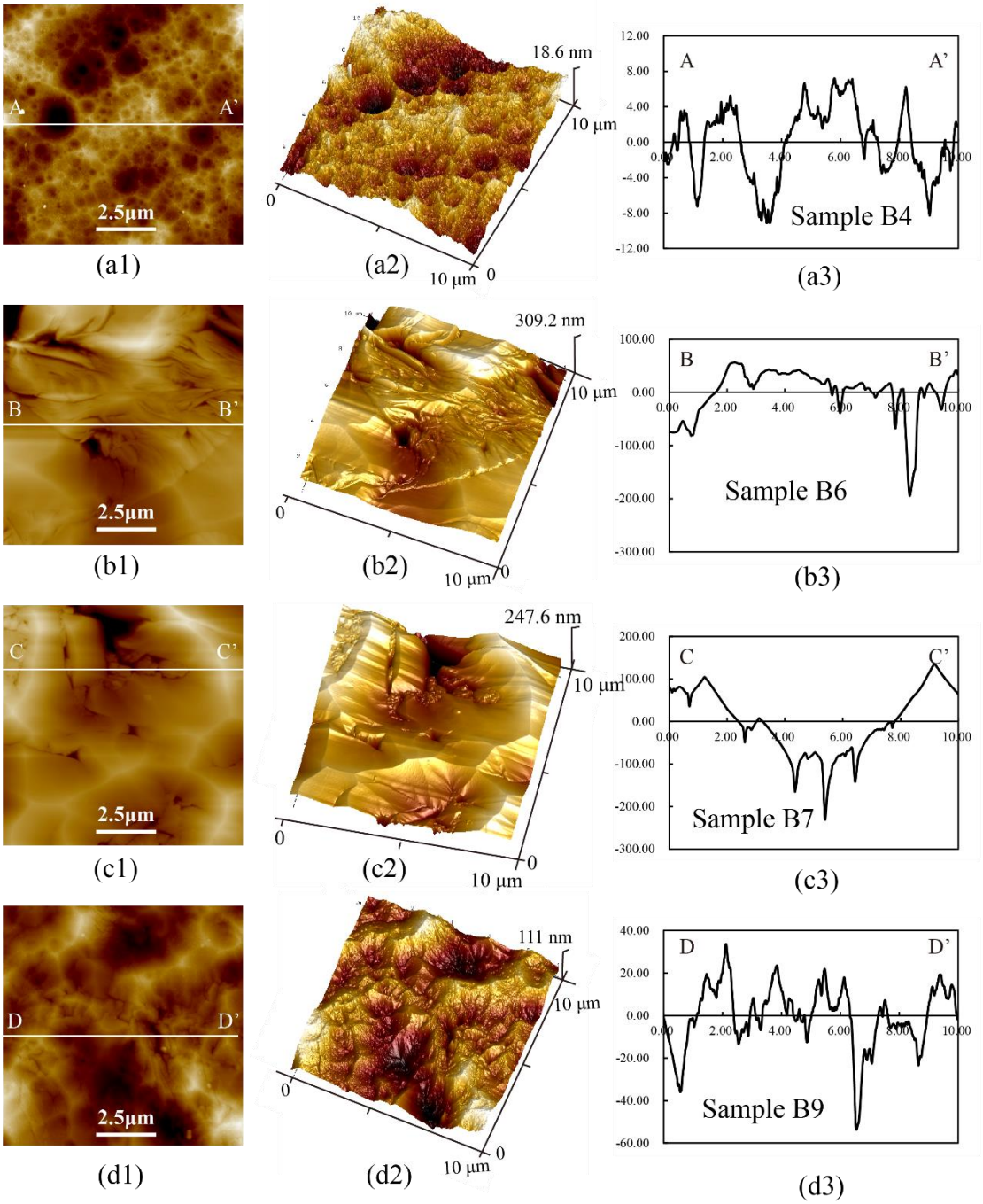

Fig. 6. Two-dimensional map, three- dimensional AFM images and section analysis. (a1-3):sample B1; (b1-3):sample B4; (c1-3): sample B5; (d1-3):sample B7

The surface roughness of the coal sample was then calculated based to the Eq (3) and Eq (4). Two separate areas are measured in single sample, 7 coals vary markedly in their mean roughness and root-mean-square roughness of surface, as presented in Table 3. There are similar results for roughness between two experiments, and values are of the same order of magnitude. R_a and R_q are in the range of 5.52-73.9 nm, and

7.85-93.5 nm respectively for the first test. R_a and R_q vary from 23.2-70.2 nm, and 27.7-92.4 nm for the second time. The R_a values are lower than R_q values, that is, R_q is more sensitive to the change of height, which is comparable to the previous research [28,51].

Table 3 The roughness of coal sample

Sample	Roughness (The first test)		Roughness (The second test)		Contact angle (°)
	R_a (nm)	R_q (nm)	R_a (nm)	R_q (nm)	
B4	5.52	7.85	23.3	27.7	52.3
B5	28.5	35.9	39	50.7	45.8
B6	21.4	28.8	24.3	31.8	52.5
B7	73.9	93.5	70.8	92.4	19.3
B8	44.5	54.4	28	34.3	43.21
B9	38.1	49.5	35.4	43.6	47.52
B10	19.2	25.8	23.2	28.2	57.19

3.3 Adhesive force of coal surface

Fig.7 (a1-c1) show adhesive force distribution (AFD) images of 3 coal samples (B1, B2 and B3) obtained by AFM, in these figures, green area represents coal matrix, red coal area pore or fracture and purple area represents mineral in coal. Fig.7 (a2-c2) present frequency distribution figures of adhesive force. Results show the adhesive force are not uniformly distributed over the whole surface of coal, in addition, there is great variation between samples in AFD, which indicated highly heterogeneous of mechanical properties of coal at micro scale[29,52]. The surface of coal commonly has two extreme frequencies, and the value of the peak varies from sample to sample as shown in Fig.7 (a1-c1). For sample B1, a narrow AFD over the range of 0–40 nN is observed, with peak at approximately 13.2 nN and 20.8 nN. While sample B2 has much wide adhesive force, which have broadened AFD in the range of -30–70 nN). In the Fig.7-b1, the adhesive force of coal matrix is 34.2 ± 5.4 nN, the adhesive force of

mineral measured by AFM is relatively high showing a 92.3 ± 10.2 nN. Furthermore, some high adhesive force appeared at the area where pore developed, that is, some pores is filled with minerals. The AFD of sample B3 shows low heterogeneous compared sample B1 and B2, and the main adhesive force is 6.5 nN and 15.9 nN, as shown in Fig.7-c2. The adhesive force of coal matrix varies greatly from a coal sample to another, which may result in the coalification.

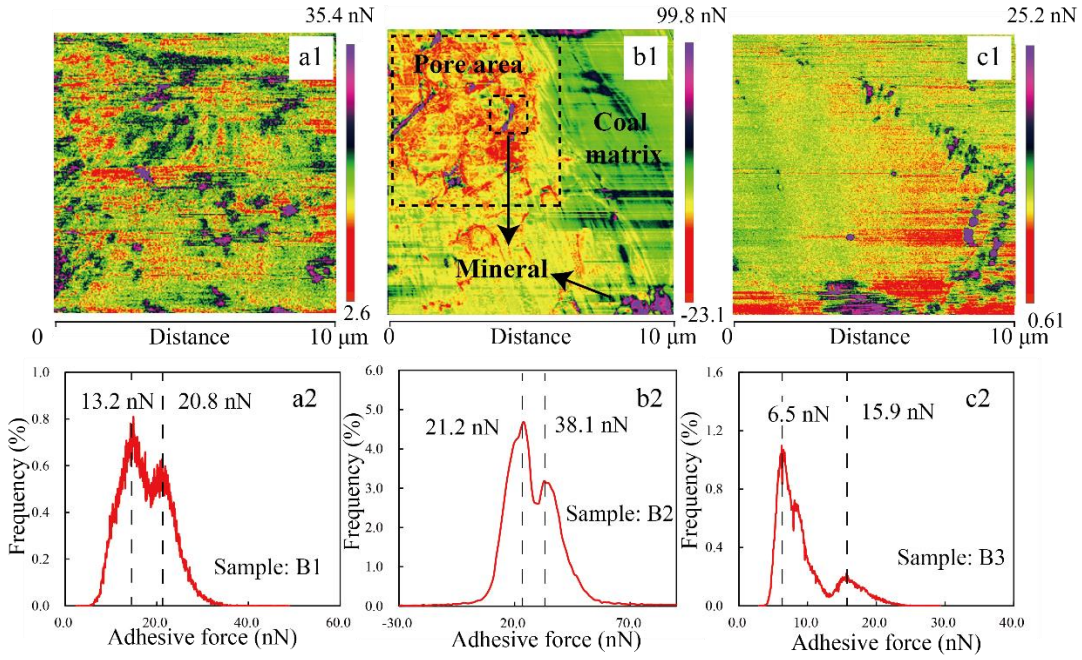

Fig.7. The adhesive force distribution of 3 coals measured by AFM.

4 Discussion

4.1 The effect of roughness on wettability

The relationship between R_a and contact angle based on Table 3 was shown in Fig.8 , in this figure, contact angle decreases linearly with increasing mean roughness for two experiments (correlation coefficient is 0.85 and 0.91, respectively), which may result from the adsorption sites for water molecule.

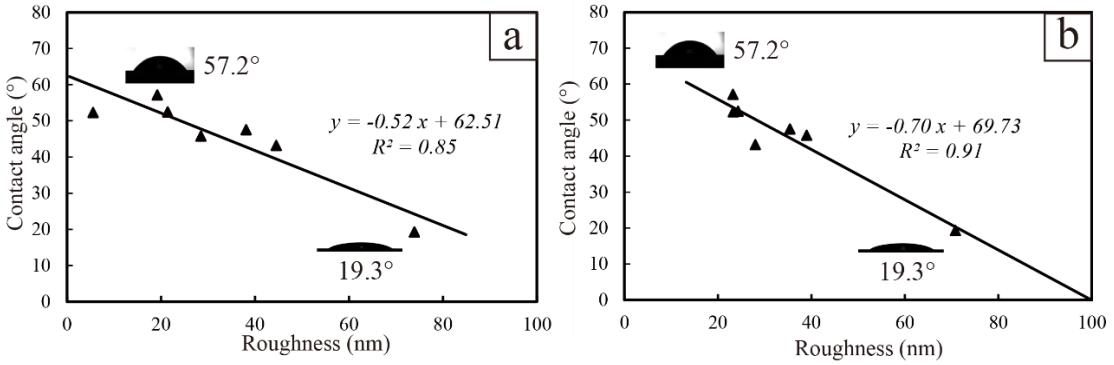

Fig. 8. Relationship between the R_a and contact angle for two experiments

The wettability of a material could be quantified by measuring the contact angle of droplet on the surface, and Yang's equation is widely used to describe the relationship between surface tension and contact angle, which could be expressed as Eq (1) however, Yang's equation is limited to ideal flat homogeneous surface. Based on energy-minimization, Wenzel modified Young's equation to account for rough surface[53,54] . In the well know Wenzel model, small gap and pore on the rough surface would be filled with liquid as shown in Fig.9b, apparent contact angle θ_m could be written as:

$$cos\theta_m = r\, cos\theta_r \quad (9)$$

Where r is roughness factor with greater than 1, θ_r is Young's contact angle.

Compared with Fig.9a, the roughness of coal surface in Fig.9b is much larger, slight surface undulation can afford enough adsorption sites for water molecules, thus more molecules can be adsorbed on the smooth pore surface, which will result in the decrease of the observed contact angle.

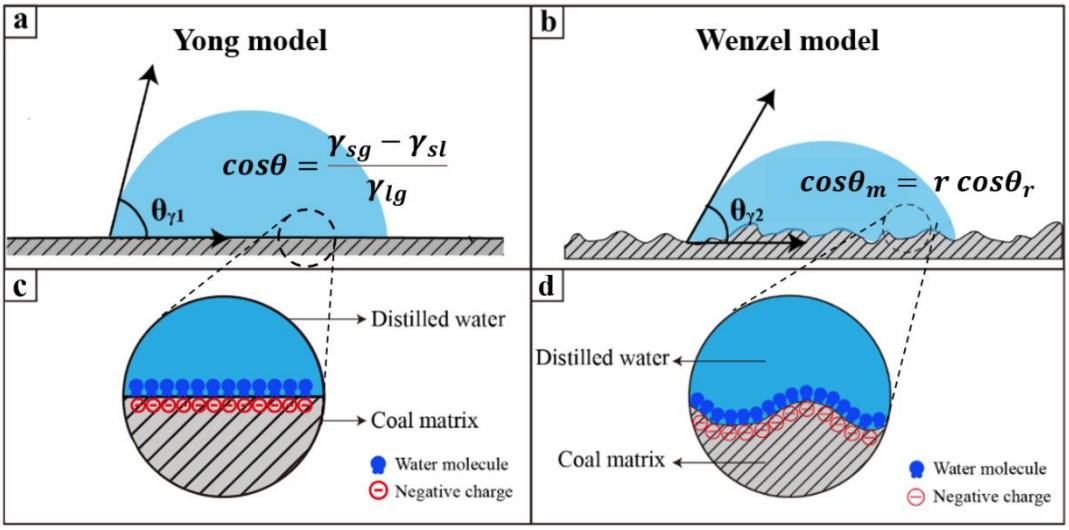

Fig. 9. Schematic representation of interfacial interaction at interface water/coal in different roughness. a- flat surface; b-rough surface; c- the schematic microscopic diagram of a; d- the schematic microscopic diagram of b.

In Wenzel's model, for hydrophilic material, rough surface would make material more hydrophilic, the larger the roughness factor is, the smaller the contact angle is, and is consistent with experiments result.

4.2 The effect of adhesive force on wettability

Coal samples used for adhesion testing shown strong hydrophilic with contact angle from 55.32°to 75.32°, and the adhesive force of micro-surface of coal has a negative linear correlation with the measured contact angles (Fig.10). As shown in this figure, a larger adhesive force of coal sample corresponds to more hydrophilic, which is related to the intermolecular force between solid and liquid.

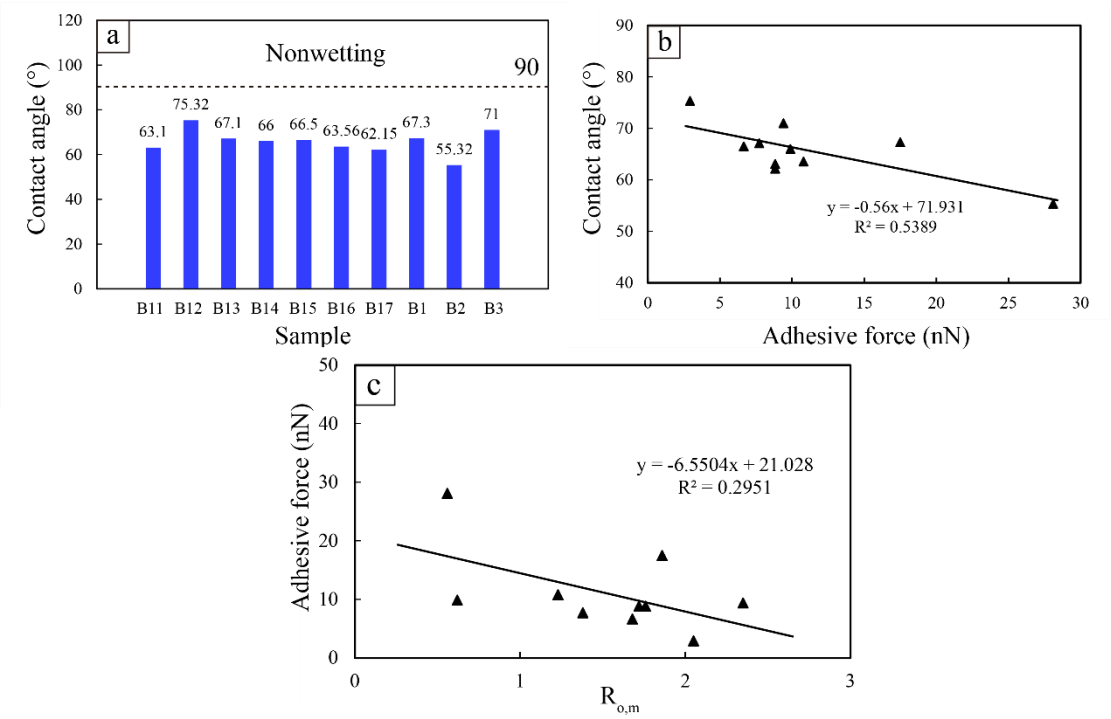

Fig. 10. (a) The wettability of coal samples and (b) the relationship between contact angle and adhesive force (c) the relationship $R_{o,m}$ and adhesive force

The average adhesive force for micro-surface varied considerably between samples, resulting from variations in the adhesive force of coal matrix of different and the distribution and content of mineral, as shown in Fig.7. The adhesive force of coal surface could reflect surface energy, which could be affected by several factors, including the structure of surface, the degree of coalification of coal and chemical composition of coal[28]. In this work, the adhesive force decline with the increase of $R_{o,m}$, that is, with the deepening of the level of coalification, intermolecular force of coal surface become weaker and result in more hydrophilic for higher rank coal, which is consistent with the results of previous study [55]. In addition, the wettability of coal would be determined some functional groups, such as $–CH_3$ and $–CH_2$ [56], however, which depends largely on oxygen-containing group for coal. There are various kind of oxygen functional groups in coal, including –OH, –OOH, –CHO, et al

[57]. Wang et al.[27] investigated the interaction between the oxygen-containing group and water molecule with molecular dynamics method, result shown hydrogen bonds and van der Waals between oxygen-containing group and water molecule are the factors that affect the wettability of coal, as shown in Fig.11, –OOH has the greatest effect on water adsorption capability, and the last one is $–OCH_3$ [27]. The difference of adhesive force is the direct consequence of functional groups in coal.

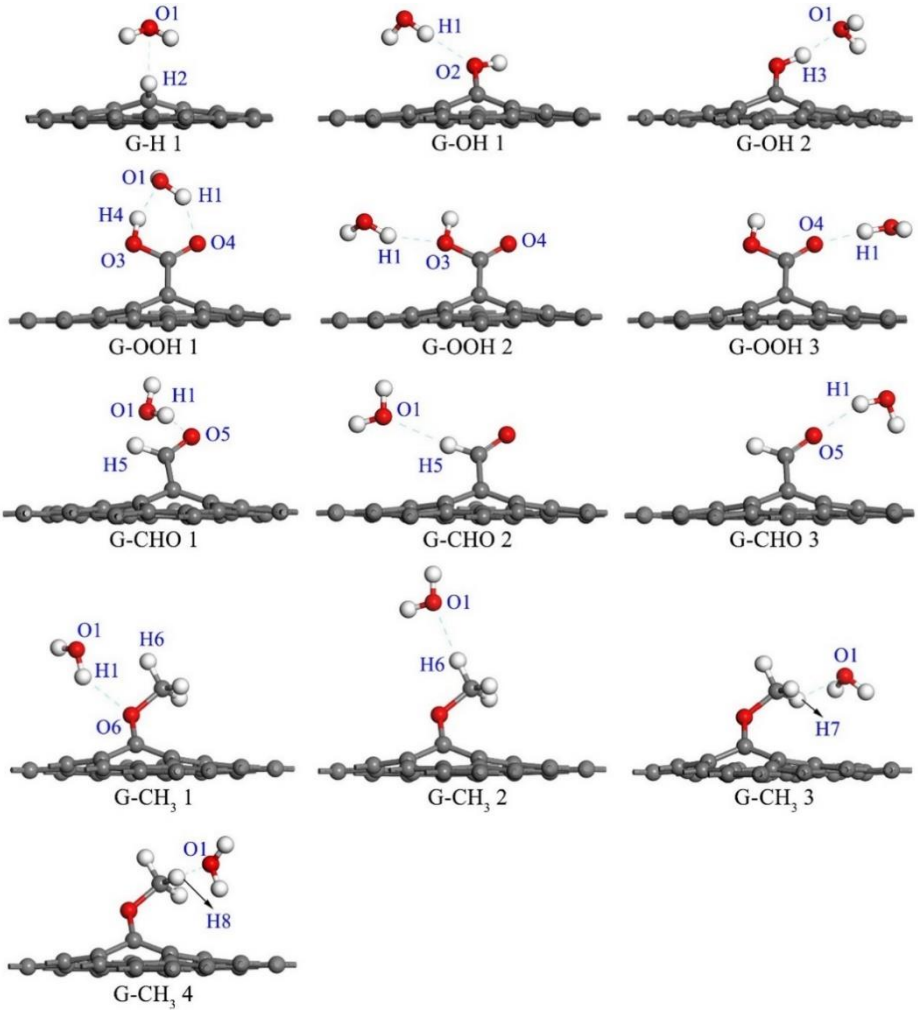

Fig.11 The interaction between the oxygen-containing group and water molecule in equilibrium from Wang[27].

Moreover, the distribution and content of minerals would greatly affect the average adhesive force of coal. Previous research shows minerals also has certain influence on

wettability. Clay mineral could promote the wettability of coal and graphite sheets mineral has negative effect on wettability due to water-depletion layer of surface[39,58]. Thus, a more hydrophilic coal, the high content of –OOH and hydrophilic mineral in coal.

4.3 The characteristic of line tension of coal

17 nanodrops were randomly selected to study the relationship between nanodrop radius and contact angle, the position and shape of nanodrops. Statistically, it was found that the contact angle of nanodroplets changed little, with the value in the range of 8°-11°. In Fig.12, we presented $\cos\theta$ as a function of $\frac{1}{r_B}$, where θ is the contact angle measured for the nanodroplet, and r_B is the radius of the droplet. As shown in this figure, there is a linear relationship between $\cos\theta$ and $\frac{1}{r_B}$. This is in line with the results from previous studies based on measurement and molecular dynamic simulations[17,31]. The modified Young's equation (Eq. 3) is then used to estimate the line tension of coal-water-air three phase contact line (2.52×10^{-11} J/m) by matching the data with a linear correlation, which is near to the result from Ma et al. based on molecular dynamics simulation [32]. which indicates that combine nanodrops vapor condensation measurements and AFM should be a reliable method to research line tension.

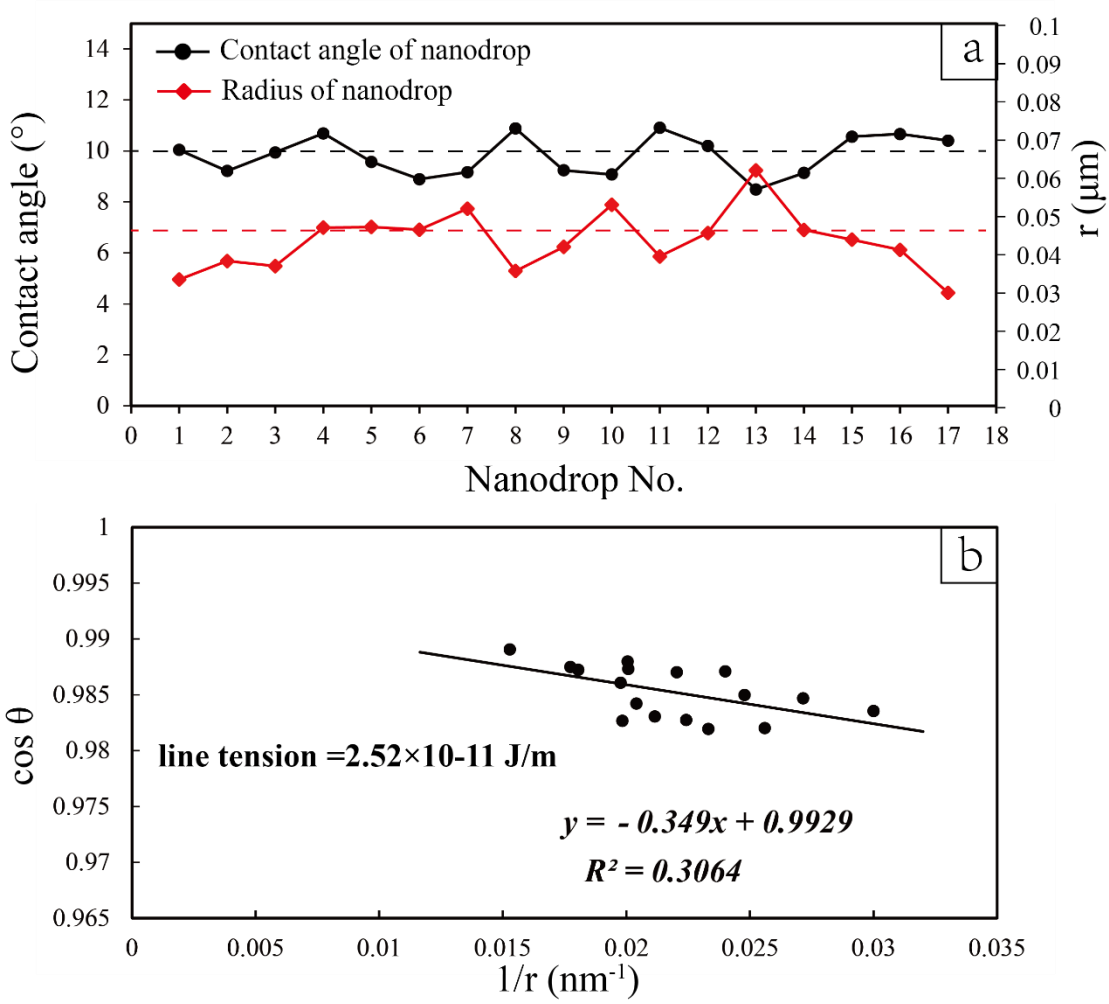

Fig. 12 (a) The contact angle and size of nanodrops. (b)The relationship between $\cos\theta$ and $\frac{1}{r}$ for nanodrops

Fig.13 shows the relationship between contact angle and drop size based on calculated line tension, drop size less than 10 nm (corresponds to micropores and mesopores in coal matrix[49]) are most heavily affected by line tension, the contact angle of nanodrops decrease from 50° to 16.67° by up to 66.67 percent, which is small change for drop size in the range of 10 nm to 100 nm (corresponds to macropores in coal matrix[49]), which indicates line tension could not be ignored when research the effect of wettability of formation water on flow-back efficiency after hydraulic fracturing in coal reservoir or numerical simulation related to capillary

force, and fluid flow behavior in fractures scarcely influenced by line tension.

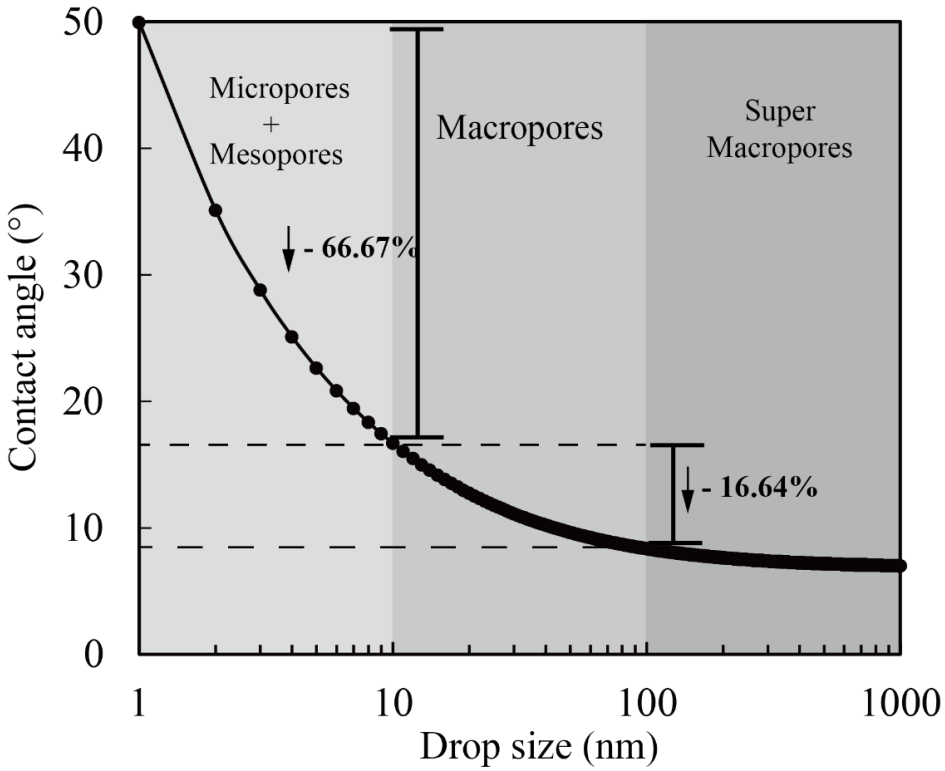

Fig.13 The relationship between contact angle and drop size

5. Conclusions

In this work, pore structures, mechanical properties and wettability of various coal samples were studied using AFM technique and the sessile drop method. Pore size and its distribution, surface topography, surface mechanical properties and how their affect wettability were researched. Moreover, line tension of coal and its influence on flow-back efficiency were discussed in detail. The major conclusions can be drawn as follows:

1) The pore size distribution of different coals has diverse variations with strong heterogeneity and micro-mesopores are mainly developed in studied coals except sample B2 and B7. AFM imaging technology could help research coal facies and

paleo-environmental conditions and provide a basis for the optimization of favorable areas in CBM reservoirs.

2) There is negative correlation between contact angle and roughness due to the adsorption sites for water molecules, slight surface undulation can afford enough adsorption sites for water molecules and result in the decrease of the observed contact angle.

3) The adhesive force of coal matrix is 34.2 ± 5.4 nN, which is smaller than mineral. The contact angle decreases with adhesive force of coal surface, which may result from the mineral and oxygen-containing group, the more hydrophilic of coal, the high content of –OOH and hydrophilic mineral in coal.

4) The line tension on the surface of coal is 2.52×10-11 J/m based on AFM image. Drop size less than 10 nm are most heavily affected by line tension, line tension could not be ignored when research the fluid flow related to capillary force in micropores and mesopores, fluid flow behavior in fractures scarcely influenced by line tension. The measurement of line tension is conducive to the study of mechanism of the wettability at nano-scale.

Acknowledgements

This research was funded by the National Natural Science Fund (grant nos. 41830427, 42130806 and 41922016), the Fundamental Research Funds for Central Universities (grant no. 2652018002), and financial support from China Scholarship Council ((No. 202006400048).

References

[1] Li Y, Yang J, Pan Z, Meng S, Wang K, Niu X. Unconventional Natural Gas Accumulations in Stacked Deposits: A Discussion of Upper Paleozoic Coal-Bearing Strata in the East Margin of the Ordos Basin, China. Acta Geol Sin - Engl Ed 2019;93:111–29. https://doi.org/10.1111/1755-6724.13767.

[2] Li Y, Zhang C, Tang D, Gan Q, Niu X, Wang K, et al. Coal pore size distributions controlled by the coalification process: An experimental study of coals from the Junggar, Ordos and Qinshui basins in China. Fuel 2017;206:352–63. https://doi.org/10.1016/j.fuel.2017.06.028.

[3] Gupta I, Rai C, Sondergeld C. Study impact of sample treatment and insitu fluids on shale wettability measurement using NMR. J Pet Sci Eng 2019;176:352–61. https://doi.org/10.1016/j.petrol.2019.01.048.

[4] Li P, Ma D, Zhang J, Tang X, Huo Z, Li Z, et al. Effect of Wettability on Adsorption and Desorption of Coalbed Methane: A Case Study from Low-Rank Coals in the Southwestern Ordos Basin, China. Ind Eng Chem Res 2018;57:12003–15. https://doi.org/10.1021/acs.iecr.8b01932.

[5] Jiao K, Yao S, Zhang K, Hu W, Cao J. The evolution of nanopores and surface roughness in naturally matured coals in South China: An atomic force microscopy and image processing study. Fuel 2018;234:1123–31. https://doi.org/10.1016/j.fuel.2018.07.102.

[6] Guo R, Kantzas A. Assessing the Water Uptake of AlbInerjetactCioonalwaitnhdLtohwe - IFmiepladctNoMf RCO2. J Can Pet Technol 2009;48:7.

[7] Donaldson EC, Thomas RD, Lorenz PB. Wettability Determination and Its Effect on Recovery Efficiency. Soc Pet Eng J 1969;9:13–20. https://doi.org/10.2118/2338-PA.

[8] Shojai Kaveh N, Rudolph ESJ, Wolf K-HAA, Ashrafizadeh SN. Wettability determination by contact angle measurements: hvbB coal–water system with injection of synthetic flue gas and CO2. J Colloid Interface Sci 2011;364:237–47. https://doi.org/10.1016/j.jcis.2011.07.091.

[9] Sun X, Yao Y, Liu D, Zhou Y. Investigations of CO2-water wettability of coal: NMR relaxation method. Int J Coal Geol 2018;188:38–50. https://doi.org/10.1016/j.coal.2018.01.015.

[10] Niu C, Xia W, Peng Y. Analysis of coal wettability by inverse gas chromatography and its guidance for coal flotation. Fuel 2018;228:290–6. https://doi.org/10.1016/j.fuel.2018.04.146.

[11] Yao Y, Liu J, Liu D, Chen J, Pan Z. A new application of NMR in characterization of multiphase methane and adsorption capacity of shale. Int J Coal Geol 2019;201:76–85. https://doi.org/10.1016/j.coal.2018.11.018.

[12] Yang J, Zhou Y. An Automatic In Situ Contact Angle Determination Based on Level Set Method. Water Resour Res 2020;56. https://doi.org/10.1029/2020WR027107.

[13] AlRatrout A, Raeini AQ, Bijeljic B, Blunt MJ. Automatic measurement of contact angle in pore-space images. Adv Water Resour 2017;109:158–69. https://doi.org/10.1016/j.advwatres.2017.07.018.

[14] Xu C, Zhou G, Qiu H. Analysis of the microscopic mechanism of coal wettability evolution in different metamorphic states based on NMR and XPS experiments. RSC Adv 2017;7:47954–65. https://doi.org/10.1039/C7RA07905B.

[15] Xue C-H, Ji P-T, Zhang P, Li Y-R, Jia S-T. Fabrication of superhydrophobic and superoleophilic textiles for oil–water separation. Appl Surf Sci 2013;284:464–71. https://doi.org/10.1016/j.apsusc.2013.07.120.
[16] Yekta-Fard M, Ponter AB. Factors affecting the wettability of polymer surfaces. J Adhes Sci Technol 1992;6:253–77. https://doi.org/10.1163/156856192X00322.
[17] Yong W, Derksen J, Zhou Y. The influence of CO2 and CH4 mixture on water wettability in organic rich shale nanopore. J Nat Gas Sci Eng 2021;87:103746. https://doi.org/10.1016/j.jngse.2020.103746.
[18] Zhao S, Li Y, Wang Y, Ma Z, Huang X. Quantitative study on coal and shale pore structure and surface roughness based on atomic force microscopy and image processing. Fuel 2019;244:78–90. https://doi.org/10.1016/j.fuel.2019.02.001.
[19] Li C, Zhang J, Han J, Yao B. A numerical solution to the effects of surface roughness on water–coal contact angle. Sci Rep 2021;11:459. https://doi.org/10.1038/s41598-020-80729-9.
[20] Wenzel RN. RESISTANCE OF SOLID SURFACES TO WETTING BY WATER. Ind Eng Chem 1936;28:988–94. https://doi.org/10.1021/ie50320a024.
[21] Zhang M, Ma L, Wang Q, Hao P, Zheng X. Wettability behavior of nanodroplets on copper surfaces with hierarchical nanostructures. Colloids Surf Physicochem Eng Asp 2020;604:125291. https://doi.org/10.1016/j.colsurfa.2020.125291.
[22] Bell MS, Borhan A. A Volume-Corrected Wenzel Model. ACS Omega 2020;5:8875–84. https://doi.org/10.1021/acsomega.0c00495.
[23] Han T-Y, Shr J-F, Wu C-F, Hsieh C-T. A modified Wenzel model for hydrophobic behavior of nanostructured surfaces. Thin Solid Films 2007;515:4666–9. https://doi.org/10.1016/j.tsf.2006.11.008.
[24] Quéré D. Rough ideas on wetting. Phys Stat Mech Its Appl 2002;313:32–46. https://doi.org/10.1016/S0378-4371(02)01033-6.
[25] Sarkar A, Kocaefe D, Kocaefe Y, Sarkar D, Bhattacharyay D, Morais B, et al. Coke–pitch interactions during anode preparation. Fuel 2014;117:598–607. https://doi.org/10.1016/j.fuel.2013.09.015.
[26] Mitchell AG, Hazell LB, Webb KJ. Wettability Determination: Pore Surface Analysis n.d.:10.
[27] Wang C, Xing Y, Xia Y, Zhang R, Wang S, Shi K, et al. Investigation of interactions between oxygen-containing groups and water molecules on coal surfaces using density functional theory. Fuel 2021;287:119556. https://doi.org/10.1016/j.fuel.2020.119556.
[28] Li Y, Yang J, Pan Z, Tong W. Nanoscale pore structure and mechanical property analysis of coal: An insight combining AFM and SEM images. Fuel 2020;260:116352. https://doi.org/10.1016/j.fuel.2019.116352.
[29] Tian X, Song D, He X, Li Z, Liu H, Wang W. Investigation on micro-surface adhesion of coals and implications for gas occurrence and coal and gas outburst mechanism. J Nat Gas Sci Eng 2021;94:104115. https://doi.org/10.1016/j.jngse.2021.104115.
[30] Weijs JH, Marchand A, Andreotti B, Lohse D, Snoeijer JH. Origin of line tension for a Lennard-Jones nanodroplet. Phys Fluids 2011;23:022001. https://doi.org/10.1063/1.3546008.
[31] Zhao B, Luo S, Bonaccurso E, Auernhammer GK, Deng X, Li Z, et al. Resolving the Apparent Line Tension of Sessile Droplets and Understanding its Sign Change at a Critical Wetting Angle. Phys Rev Lett 2019;123:094501. https://doi.org/10.1103/PhysRevLett.123.094501.

[32] Ma X, Dong X, Fan Y. Prediction and Characterization of the Microcrystal Structures of Coal with Molecular Simulation. Energy Fuels 2018;32:3097–107. https://doi.org/10.1021/acs.energyfuels.7b03698.
[33] Emmanuel S, Eliyahu M, Day-Stirrat RJ, Hofmann R, Macaulay CI. Softening of organic matter in shales at reservoir temperatures. Pet Geosci 2017;23:262–9. https://doi.org/10.1144/petgeo2016-035.
[34] Koetniyom W, Suhatcho T, Treetong A, Thiwawong T. AFM force distance curve measurement for surface investigation of polymers compound blend with metal nanoparticles. Mater Today Proc 2017;4:6205–11. https://doi.org/10.1016/j.matpr.2017.06.117.
[35] Luo Y, Andersson SB. A continuous sampling pattern design algorithm for atomic force microscopy images. Ultramicroscopy 2019;196:167–79. https://doi.org/10.1016/j.ultramic.2018.10.013.
[36] Kulkarni T, Tam A, Mukhopadhyay D, Bhattacharya S. AFM study: Cell cycle and probe geometry influences nanomechanical characterization of Panc1 cells. Biochim Biophys Acta BBA - Gen Subj 2019;1863:802–12. https://doi.org/10.1016/j.bbagen.2019.02.006.
[37] Li Y, Chen J-Q, Yang J-H, Liu J-S, Tong W-S. Determination of shale macroscale modulus based on microscale measurement: A case study concerning multiscale mechanical characteristics. Pet Sci 2021:S1995822621000996. https://doi.org/10.1016/j.petsci.2021.10.004.
[38] Pan B, Li Y, Xie L, Wang X, He Q, Li Y, et al. Role of fluid density on quartz wettability. J Pet Sci Eng 2019;172:511–6. https://doi.org/10.1016/j.petrol.2018.09.088.
[39] Lu Y, Liu D, Cai Y, Li Q, Zhou Y. Spontaneous imbibition in coal with in-situ dynamic micro-CT imaging. J Pet Sci Eng 2022;208:109296. https://doi.org/10.1016/j.petrol.2021.109296.
[40] Boruvka L, Neumann AW. Generalization of the classical theory of capillarity. J Chem Phys 1977;66:5464–76.
[41] Yao Y, Ren L, Gao S, Li S. Histogram method for reliable thickness measurements of graphene films using atomic force microscopy (AFM). J Mater Sci Technol 2017;33:815–20. https://doi.org/10.1016/j.jmst.2016.07.020.
[42] Jafarzadegan K, Merwade V. A DEM-based approach for large-scale floodplain mapping in ungauged watersheds. J Hydrol 2017;550:650–62. https://doi.org/10.1016/j.jhydrol.2017.04.053.
[43] Yang F, Ning Z, Wang Q, Zhang R, Krooss BM. Pore structure characteristics of lower Silurian shales in the southern Sichuan Basin, China: Insights to pore development and gas storage mechanism. Int J Coal Geol 2016;156:12–24. https://doi.org/10.1016/j.coal.2015.12.015.
[44] Shen R, Xiong W, Lang X, Wang L, Guo H, Zhou H, et al. Quantitative analysis of nano-scale pore structures of broad sense shale oil reservoirs using atomic force microscopy. Energy Explor Exploit 2021;39:1839–56. https://doi.org/10.1177/01445987211022522.
[45] Wang S, Liu S, Sun Y, Jiang D, Zhang X. Investigation of coal components of Late Permian different ranks bark coal using AFM and Micro-FTIR. Fuel 2017;187:51–7. https://doi.org/10.1016/j.fuel.2016.09.049.
[46] Everson I, Bendall B, Murray A. Otolith and body size relationships in the mackerel icefish

(Champsocephalus gunnari). CCAMLR Sci 1999;6:117–23.
[47] Trtik P, Kaufmann J, Volz U. On the use of peak-force tapping atomic force microscopy for quantification of the local elastic modulus in hardened cement paste. Cem Concr Res 2012;42:215–21. https://doi.org/10.1016/j.cemconres.2011.08.009.
[48] Eliyahu M, Emmanuel S, Day-Stirrat RJ, Macaulay CI. Mechanical properties of organic matter in shales mapped at the nanometer scale. Mar Pet Geol 2015;59:294–304. https://doi.org/10.1016/j.marpetgeo.2014.09.007.
[49] Cai Y, Liu D, Pan Z, Yao Y, Li J, Qiu Y. Pore structure and its impact on CH4 adsorption capacity and flow capability of bituminous and subbituminous coals from Northeast China. Fuel 2013;103:258–68. https://doi.org/10.1016/j.fuel.2012.06.055.
[50] Loucks RG, Reed RM, Ruppel SC, Hammes U. Spectrum of pore types and networks in mudrocks and a descriptive classification for matrix-related mudrock pores. AAPG Bull 2012;96:1071–98. https://doi.org/10.1306/08171111061.
[51] Liu J, Jiang X, Huang X, Wu S. Morphological characterization of super fine pulverized coal particle. Part 2. AFM investigation of single coal particle. Fuel 2010;89:3884–91. https://doi.org/10.1016/j.fuel.2010.07.001.
[52] Shi X, Pan J, Hou Q, Jin Y, Wang Z, Niu Q, et al. Micrometer-scale fractures in coal related to coal rank based on micro-CT scanning and fractal theory. Fuel 2018;212:162–72. https://doi.org/10.1016/j.fuel.2017.09.115.
[53] Good RJ. A Thermodynamic Derivation of Wenzel's Modification of Young's Equation for Contact Angles; Together with a Theory of Hysteresis [1]. J Am Chem Soc 1952;74:5041–2. https://doi.org/10.1021/ja01140a014.
[54] Whyman G, Bormashenko E, Stein T. The rigorous derivation of Young, Cassie–Baxter and Wenzel equations and the analysis of the contact angle hysteresis phenomenon. Chem Phys Lett 2008;450:355–9. https://doi.org/10.1016/j.cplett.2007.11.033.
[55] Wu S, Tang D, Li S, Meng Y, Lin W. Evaluation of pore development in different coal reservoirs based on centrifugation experiment. J Pet Sci Eng 2017;157:1095–105. https://doi.org/10.1016/j.petrol.2017.08.027.
[56] Guanhua N, Zhao L, Qian S, Shang L, Kai D. Effects of [Bmim][Cl] ionic liquid with different concentrations on the functional groups and wettability of coal. Adv Powder Technol 2019;30:610–24. https://doi.org/10.1016/j.apt.2018.12.008.
[57] Xin H, Wang D, Qi X, Qi G, Dou G. Structural characteristics of coal functional groups using quantum chemistry for quantification of infrared spectra. Fuel Process Technol 2014;118:287–95. https://doi.org/10.1016/j.fuproc.2013.09.011.
[58] Xia Y, Xing Y, Li M, Liu M, Tan J, Cao Y, et al. Studying interactions between undecane and graphite surfaces by chemical force microscopy and molecular dynamics simulations. Fuel 2020;269:117367. https://doi.org/10.1016/j.fuel.2020.117367.